This is a repository copy of *Hydrogen production from cellulose catalytic gasification on CeO<inf>2</inf>/Fe<inf>2</inf>O<inf>3</inf>catalyst*.

Article:

Hydrogen production from cellulose catalytic gasification on CeO_2/Fe_2O_3 catalyst

Jun Zou[a], Japhet Oladipo[b], Shilong Fu[a], Amal Al-Rahbi[b], Haiping Yang[a*], Chunfei Wu[c*], Ning Cai[a], Paul Williams[b], Hanping Chen[a]

[a] State Key Laboratory of Coal Combustion, Huazhong University of Science and Technology, Wuhan, 430074, China

[b] School of chemical and process engineering, SCAPE, The University of Leeds, Leeds, LS2 9JT, UK

[c] School of Engineering, University of Hull, Hull, HU6 7RX, UK

* Corresponding author (H. Yang). Tel.: +86 27 87542417.   Email: yhping2002@163.com

** Corresponding author (C. Wu),. Tel.: +44 1133432504.   Email: C.Wu@hull.ac.uk

Abstract

Catalytic steam gasification of biomass can produce clean and renewable hydrogen. In this study, Ce/Fe bimetallic catalysts were used to promote hydrogen production from cellulose steam catalytic reforming at 500-900 ^{o}C. The effect of different Ce/Fe ratios on the catalytic performance of hydrogen production was studied. The distribution of products, gas composition, carbon deposition and the stability of the catalyst were analyzed with variant approaches. The results show that the catalytic performance of the CeO_2/Fe_2O_3 catalyst in relation to hydrogen production was much better than pure CeO_2 or Fe_2O_3. When the ratio of Ce:Fe was 3:7, the maximum yield of the H_2 was 28.58 mmol at 800 ^{o}C. $CeFeO_3$ could be generated at 800 ^{o}C or higher temperature

23   after redox reactions without forming CeO_2/Fe_2O_3 clathrate. And the existence of

24    $CeFeO_3$ enhanced the thermal stability of Ce/Fe catalyst. The presence of CeO_2 not

25   only improved the oxidative ability of the iron catalysts, but also was in favour of the

26   oxidation of possible deposited carbon on the surface of the used catalysts.

28

29

30   Graphic abstract
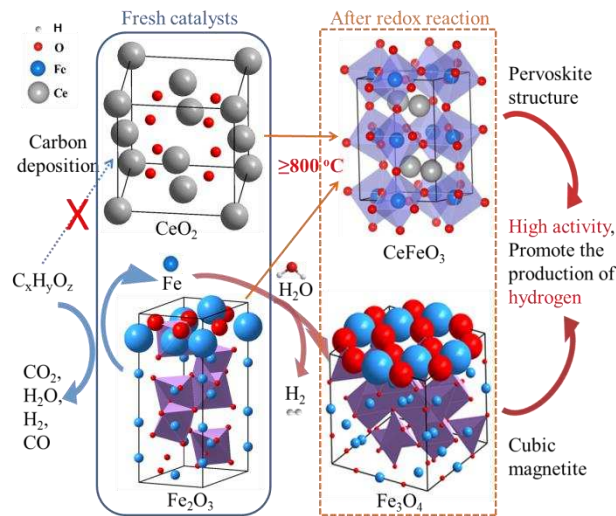
31

32   Schematic of cellulose gasification process with CeO_2/Fe_2O_3. After redox reaction,

33   high active phases like $CeFeO_3$ and Fe_3O_4 were generated.

34   1. Introduction

35   Hydrogen is a renewable and clean energy carrier and its application only

36   generates water [1, 2]. Currently, the production of hydrogen is mainly from the

37   processing of fossil fuels such as coal gasification and natural gas reforming. The use

38   of fossil fuels results in the generation of greenhouse gases which are responsible for

39   climate change. Hence, renewable and sustainable feedstocks such as biomass have

40   drawn increasing attention [3, 4]. Converting renewable biomass into hydrogen can be

41   processed through steam catalytic gasification [5-8].

42   However, there are many challenges for catalytic biomass gasification. For

43   example, the content of alkali metals in biomass is very high, which could be

44   evaporated at high temperature and cause corrosion and agglomeration issues [9].

45   Another challenge of catalytic biomass gasification is that heavy tar compounds

46   produced from thermal-chemical conversion of biomass can cause coke deposition on

47   the surface of catalysts. Considering those two issues, a two-stage pyrolysis-catalytic

48   steam reforming is proposed and applied [10, 11]. In the two-stage process of biomass

49   gasification, the pyrolysis of biomass happens at the first stage. And the derived

50   vapours from biomass gasification are catalytic reformed to produce hydrogen with

51   catalyst in the second stage. Therefore, the catalytic stage can be separately controlled

52   with flexible manipulation of process parameters [12, 13]. In addition, the poisoning

53   of catalyst caused by the contaminants from biomass pyrolysis can be limited [14].

54   Apart from the process optimisation of biomass gasification, catalyst plays an

55   important role in tar conversion and promoting hydrogen production [10, 11, 14].

56   Generally, metallic catalysts like nickel or iron based materials perform well in the

57   thermochemical conversion processes as widely reported [14-17]. Although Fe-based

58   catalysts offer relatively low activity than Ni, Fe is not toxic and much cheaper.

59   Therefore, it has high economic feasibility potentials in biomass gasification [18-21].

60   Furthermore, to reach the goal of turning the gas products into hydrogen enriched

61   syngas, steam as the gasification oxidant agent is necessary and water gas shift

62   reaction (WGS) is applied [22-25]. It is known that the efficient catalytic metal for

63   WGS is Fe_3O_4 [24, 26, 27].

64   However, iron catalyst has some disadvantages mainly caused by thermal sintering

65   of the active phase Fe_3O_4 at high gasification temperature [27]. Another problem of

66   iron catalyst deactivation is caused by the over-reduction of Fe_2O_3 to metallic iron and

67   even iron carbides [28], while the metallic Fe is beneficial for Fischer-Tropsch [29]

68   and methanation reactions but not helpful to WGS process [30, 31]. So metal oxides

69　　supporters like Al_2O_3, Cr_2O_3, ZrO_2 or SiO_2 were introduced into the iron oxides to

70　　decrease the sintering and enhance the material stability [32]. In the tar reforming

71　　experiments, Kell found that the mixture of La and Fe with ZrO_2 as support show high

72　　catalytic activity in benzene cracking [21]. While Kang pointed out that the

73　　introducing of copper to Fe_3O_4 increased the reduction kinetics and inhibited the

74　　carbon deposition and Fe_3C formation during methane reforming [30]. Khan

75　　introduced several metal ions into the iron oxide and found that the influencing effect

76　　strongly rely on the nature of addition of metal cations, and Fe/Ce could approach

77　　equilibrium conversion during high temperature water gas shift reaction, and ceria

78　　exhibits a synergetic effect on the performance of iron oxide [27]. On the one hand,

79　　some of the researchers focus on the small amount of CeO_2 with some other metal

80　　oxide as a promoter for tar reforming [16, 17, 22]. Laosiripojana suggested that the

81　　$GdCeO_2$ coating over $NiFe/MgOAl_2O_3$ performed much better in naphthalene steam

82　　reforming [16]. Chen found that $La_{0.8}Ce_{0.2}FeO_3$ catalyst showed better activity and

83　　stability than commercial Ni/Al_2O_3 during bio-oil/bioslurry steam gasification [22].

84　　On the other hand, to prevent the over-reduction of iron oxide, high capacity and

85　　mobility of oxygen is essential to improve the oxidative ability of the iron catalysts,

86　　and high Ce:Fe ratio catalyst was usually used for oxygen carrier in redox reaction.

87　　Lee found that Fe-based mediums with 30 wt% of CeO_2 exhibited high activity and

88　　stability in water splitting oxidation for chemical hydrogen storage [33]. And Fe/Ce

89　　performed well in Reddy's the long-term water gas shift reaction experiments.

90　　Yamaguchi also pointed out that CeO_2 was an effective modification of Fe_2O_3 and

91   improved the thermal stability during the methane-steam redox process [34]. However,

92   biomass steam gasification is much more complex than oil model compounds

93   gasification and water-gas shift or other simple gas like methane steam reforming; it

94   includes all above reactions and is consisted of volatile releasing, cracking and

95   derived gases steam reforming. So the influence of Ce/Fe catalyst in biomass steam

96   gasification should be explored.

97   In addition, the application about perovskite structure(ABX3) in photochemical

98   reactions has been drawn more and more attentions since it was rated the top 10

99   scientific breakthroughs by the editors Science [35] and Nature [36] in 2013.

100   Moreover, relatively high ratio of CeO_2 in Ce/Fe catalyst has been synthesised into

101   $CeFeO_3$, whose perovskite structure exhibits not only high photocatalytic activity [37],

102   but also high capacity and mobility of oxygen, which means that it is potential to be

103   used in redox process [38-40]. Manwar revealed that nanocrystalline $CeFeO_3$ is a

104   potential candidate for photo-electrochemical water splitting reaction [41]. However

105   they are seldom studied in thermal-chemical reactions. Recently, Sahoo synthesized 3

106   or 6 at.% Fe-doped CeO_2 with microwave assisted combustion method and found that

107   they could be used for both CO oxidation and soot combustion, and exhibited high

108   thermal stablitity [42]. Ce/Fe binary catalysts have been studied by introducing high

109   ratio of ceria into the catalyst to forming $CeFeO_3$ rather than acting as catalyst

110   supporter or promoter. In addition, these catalysts were used mainly for

111   photochemical reaction rather than for biomass steam gasification. This paper uses

112   high photocatalytic active phase of $CeFeO_3$ for biomass steam gasification.

113   Thereby, in this study, Ce/Fe catalyst was introduced into biomass steam

114   gasification and optimizing the mole ratio of cerium to iron is studied, in relation to

115   the yield of hydrogen production and the stability of catalyst using a two-stage reactor.

116   Temperature programmed reduction/oxidation (TPR/TPO) and X-Ray Diffractometer

117   (XRD) were applied to investigate the formation of $CeFeO_3$ and the mechanism of the

118   CeO_2/Fe_2O_3 catalysts on biomass gasification.

119

120   2. Experimental material and methods

121   2.1 Biomass materials and catalyst preparation

122   Cellulose (microcrystalline powders of 20 μm particle size, Sigma-Aldrich Co.,

123   Ltd.) was applied as a representative material of biomass feedstock. Proximate and

124   ultimate analysis of the cellulose sample can be found in our previous work [43]. The

125   TGA analysis showed that cellulose began to decompose at about 310 ^{o}C and was

126   entirely converted at 450 ^{o}C, as shown in supplementary materials Fig.1S.

127   A wet impregnation method was applied for the preparation of CeO_2/Fe_2O_3

128   catalysts. CeO_2 (analytically pure, Sigma-Aldrich Co., Ltd.) was impregnated with

129   aqueous solution of $Fe(NO_3)_3 \cdot 9H_2O$ (analytically pure, Sigma-Aldrich Co., Ltd.). The

130   catalyst precursors were kept stirring at 80 ^{o}C for 6h and dried at 105 ^{o}C overnight,

131   and subsequently calcined at 800 ^{o}C for 4h in a muffle furnace under air atmosphere.

132   Then the catalysts were crushed and sieved to granules with the size ranging from

133   0.245 to 0.350 mm prior to experimental work. While the raw CeO_2 and Fe_2O_3

134   (analytically pure, Sigma-Aldrich Co., Ltd.) were used directly as catalysts for

135   comparison. The catalysts were not reduced prior to the experiment since the derived

136   gases during pyrolysis-gasification process like hydrogen and carbon monoxide can

137   reduce the metal oxides in situ. Different mole ratios of Ce/Fe in CexFeyO were

138   prepared as X:Y=1:0, 7:3, 5:5; 3:7; 0:1. The actual ratios of Ce:Fe after the

139   preparation of catalysts were detected by ICP-MS (ELAN DRC-e, PerkinElmer,

140   America), and the related results were listed in Table 1S. The blank experiment

141   without any catalysts was assigned as "w/o".

142

143   2.2 Experiment apparatus and method

144   The gasification of cellulose sample was performed in a two stage pyrolysis

145   catalytic reforming fixed-bed system as shown in Fig. 1, which is consisted of

146   two-stage fixed-bed furnace with two temperature ranges (First stage: pyrolysis zone;

147   Second stage: gasification zone; the height of both is 310 mm), a quartz tube reactor

148   with an internal diameter of 45 mm, water feeding system, cooling system filled with

149   water/ice mixture, as well as gas cleaning system following by gas collecting and

150   measuring system.

151   For each experiment, 1 g CeO_2/Fe_2O_3 catalyst, embraced by quartz wool, was put

152   on a porous plate in the second reactor. The carrier gas (Nitrogen, 99.999%) was kept

153   as 300 ml min^{-1}. Then the first stage was set at 800 $^{\circ}$C for cellulose pyrolysis, while

154   the gasification temperature varied from 500 $^{\circ}$C to 900 $^{\circ}$C with the step of 100 $^{\circ}$C.

155   When the pyrolysis and gasification reactors were heated and stabilized at set

156   temperatures, respectively, 2 g cellulose (supported by silica wool, in a quartz basket

157   with an internal diameter of 28 mm) was fed into the first reactor. At the same time, a

158   precise syringe pump introduced the water at 0.1 g min^{-1} through a stainless steel tube

159   which passed the pyrolysis stage and reached the entrance of gasification reactor for

160   catalytic steam reforming. Fast pyrolysis of cellulose sample happened in the first

161   stage and the derived pyrolyzed volatiles were catalytic steam reformed at the second

162   stage in the presence of the CeO_2/Fe_2O_3 catalyst. After the pyrolysis and catalytic

163   reforming, the outlet products passed through two condensers with water ice mixture,

164   where the water and condensable vapors were collected. Finally, the noncondensable

165   gases were cleaned, dried and sampled with a gas bag. The gas sample was collected

166   every two minutes for detecting the gas content. It turned out that the effective gases

167   like CO, H_2, CO_2 and CH_4 were below detection limit after 40 minutes, so it can be

168   sure that the reaction was completed and all the products were collected. Each

169   experiment was performed for 40 minutes and every gas sample was tested for three

170   times at least and the results were averaged.

171
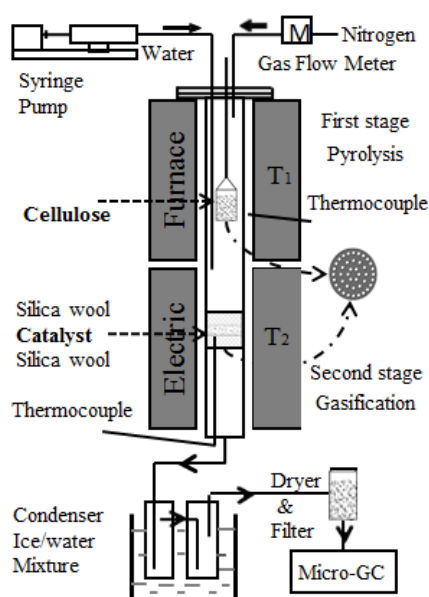
172

173   Figure 1. Schematic diagram of the reactor system

174   2.3 Characterizations of gas products and catalysts

175   Gas sample collected in the gas bag was analyzed off-line with a gas

176   chromatography (GC) (Panna A91, China). The produced gas sample was analyzed

177   using a dual channel GC with a thermal conductivity detector (TCD) and a flame

178   ionization detector (FID). Column A was Porapak Q (He as carrier gas) for the

179   analysis of CO_2 at 80°C. Column B was 5A zeolite molecular sieve (MS-5A, He as

180   carrier gas) for the measurement of H_2, N_2, O_2, CO, CH_4 at 100°C. The N_2

181   concentration and flow rate were used as the tracer to calculate the mass of each gas

182   (in volume, at 1 atm and 25°C). The total yield of gas production and liquid

183   production were calculated by the obtained mass of gas and liquid in relation to the

184   weight of cellulose sample. And the variation of char yield can be neglected since the

185   pyrolysis stage was carried out at the same condition at each experiment and the

186   weight of residual solid char ranged from 0.119 g to 0.121 g. While the mass balance

187   was calculated by that the whole productions of gas, liquid and char divided by the

188   total weight of input including cellulose and steam. For each test, it was repeated at

189   least three times, the repeatability was kept above 95%, and the results were averaged.

190   In order to investigate the stability performance of the catalysts during the cellulose

191   gasification, life time test was carried out. After each experiment, the catalyst was

192   kept in the furnace without any other changing while just the fresh cellulose sample

193   was introduced. So the used catalyst was recycled for the cellulose catalytic

194   gasification.

195   The crystal structure of the fresh and used catalysts was characterized by X-Ray

196   Diffractometer (XRD, X'Pert PRO, PANalytical B.V, Netherlands) with Cu Kα

197   radiation (λ=1.5406 Å) operating at 40KV and 40mA at 2θ range between 10 and 85°.

198   PANalytical X'pert HighScore software was used to analyse the diffraction spectra

199   peaks and the reference data from the Joint Committee on Powder Diffraction

200   Standard (JCPDS) files was applied to identify the crystal phases existed in the

201   samples.

202   The reducibility of the catalysts was characterized with Hydrogen temperature

203   programmed reduction method (H_2-TPR) using a Catalyst Analyzer (Belcat-M,

204   Microtrac BEL., Corp). Before the reduction, 100 mg catalyst was heated from room

205   temperature to 500 °C at a heating rate of 10 °C min^{-1} and kept isothermal for 1h, then

206   cooled down to 100 °C. In the above process, High purity argon (99.999%) was used

207   as purging gas. After that the gas was switched to 5% H_2/Ar (30 cm^3 min^{-1}), the TPR

208   test was carried out from 100 °C to 800 °C at a heating rate of 10 °C min^{-1} and kept

209   for 30 minutes. An on-line thermal conductivity detector (TCD) was applied to

210   measure the consumption of hydrogen [44].

211   In order to investigate the properties of used catalysts and the possible deposited

212   carbon on the surface, temperature programmed oxidation (TPO) was carried out in a

213   thermogravimetric analyser (Labsys Evo1150, Setaram instrumentation, France). 30

214   mg reacted catalyst was heated to 105 °C and kept for 20 minutes, then it was heated

215   up to 850 °C at 10 °C min^{-1}, and holding for 20 minutes. A high resolution scanning

216   electron microscope (SEM, Quanta 200, FEI, Netherlands) was applied to test the

217   surface morphology of the used catalysts.

218   3. Results and discussion

219   3.1. Influence of the ratio of Ce:Fe

220   3.1.1. Gas distribution

221   To investigate the influence of the ratio of Ce:Fe on the cellulose steam

222   gasification, pure CeO_2 or Fe_2O_3 and different mole ratios of Ce:Fe (7:3, 5:5, 3:7)

223   were introduced into the catalytic stage. Both pyrolysis stage and gasification stage

224   were set at 800 °C. And the feeding rate of water was kept at 0.1 g min^{-1}. Since the

225   reaction time was 40 min, the total water introduced into the system was 4 g, which

226   far surpassed the content of tar in the liquid product (water and tar were both

227   condensed in the condenser), the characteristics of oil was not analyzed here. And the

228   weight of residual solid char was steady from 0.119 g to 0.121 g, which indicated that

229   the variation of char yield could be neglected since the pyrolysis stage was carried out

230   at the same condition for each trial. While the total yield of gas production was

231   calculated with the mass of gas in relation to the weight of cellulose sample. And the

232   product yield and gas distribution of cellulose gasification with variant Ce/Fe catalyst

233   are shown in Table 1. The mass balance was calculated by that the whole productions

234   of gas, liquid and char divided by the total weight of input including cellulose and

235   steam, and its' value ranged from 96.54% to 100.15%, it indicated that the experiment

236   results were reliable. Under the condition that without any catalysts were used, the gas

237   yield was 71.53 wt%, while the yield and content of hydrogen were 13.88 mmol g^{-1}

238   cellulose and 23.07 vol.% separately, the values of them were low. When CeO_2 was

239   introduced, the gas yield was decreased slightly from 71.53 wt.% to 70.45 wt.% but

240   the yield of hydrogen was increased slightly to 15.65 mmol g^{-1} cellulose, while the

241   content of CO_2 decreased sharply and the content of CO increased significantly, this might be

242   attributed to that CeO_2 prevented the further conversion of oil and the water gas shift. In

243   regard to Fe_2O_3 addition, the same tendency was showed with that of CeO_2. The CO content

244   increased up to 53.07 vol.% at the price of CO_2 diminishing to 10.42 vol.%. The content of H_2

245   was decreased slightly from 23.07 vol.% to 22.05 vol.%, while the yield of hydrogen

246   increased to 17.30 mmol g^{-1} cellulose. However, the gas yield under Fe_2O_3 increased largely

247   to 87.13% which is much higher than that of CeO_2. It indicated that Fe_2O_3 performed

248   important role in promoting the thermal cracking and steam reforming of tar into light gases.

249   In general, the yield of combustible gases (H_2, CO, CH_4) increased when CeO_2 or

250   Fe_2O_3 was introduced. And the low heating value was 13.55 MJ $(Nm^3)^{-1}$ and 14.27MJ

251    $(Nm^3)^{-1}$ respectively.

252   The yield of gas product with CeO_2/Fe_2O_3 mixture was shown in Table 1. With the

253   ratio of Fe increasing, the concentration of CO increased slightly from 49.15 vol.% to

254   53.07 vol.% (the yield of CO was increased by 34.5% from 30.97 mmol to 41.64

255   mmol correspondingly, refer to Fig.2S), CH_4 showed similar trend as the content of

256   CH_4 was increased slightly from 12.99 vol.% to 14.45 vol.%, while the CO_2

257   concentration decreased from 13.00 vol.% to 10.42 vol.%. It is suggested that the

258   introduction of Fe promoted the thermal cracking of the pyrolysis volatiles resulting

259   in the increase of the production of CO and CH_4. It should be noticed that when the

ratio of Ce:Fe was decreased gradually from 1:0 (pure CeO_2) to 0:1 (pure Fe_2O_3), the concentration of H_2 and CO_2 were increased initially and then reduced, while the concentration of CO was decreased at first and then increased. Those might be related to reverse water gas shift (RWGS, $CO_2 + H_2 = CO + H_2O$, $\Delta H = +41.19$ KJ mol^{-1}), which was endothermic reaction. It is proposed that the reverse water gas shift at 800 ^{o}C was enhanced, which restrained the production of H_2 and CO_2. The maximum yield of hydrogen (28.58 mmol, more than twice of without catalyst) was obtained at the Ce:Fe ratio of 3:7. It indicatesd that the ratio of 3:7 (Ce:Fe) is the optimal value for the hydrogen production in this work, much better than that of pure CeO_2 or Fe_2O_3. It might be owing to that ceria and iron shows synergy in volatile conversion and hydrogen production.

Table.1 Gas yields under different mole ratios of Ce:Fe.

Different Ce:Fe ratio	w/o	CeO_2	Ce:Fe=7:3	Ce:Fe=5:5	Ce:Fe=3:7	Fe_2O_3
Gas yield (wt.%)	71.53	70.45	74.36	83.79	84.64	87.13
Mass balance (%)	98.74	100.15	96.54	98.90	98.30	98.28
H_2 yield (mmol g^{-1} cellulose)	13.88	15.65	21.70	27.01	28.58	17.30
Gas composition (vol.%)						
H_2	23.07	24.85	30.38	32.53	33.69	22.05
CO_2	20.57	13.00	13.70	12.77	12.12	10.42
CH_4	12.79	12.99	12.65	13.20	10.93	14.45
CO	43.58	49.15	43.27	41.50	43.26	53.07

3.1.2. XRD analysis

Fig. 2 shows the X-ray diffraction patterns of the fresh and reacted catalysts with different Ce:Fe ratios prepared by impregnation. It shows that the main crystal phases in the fresh catalysts were the same, it mainly includes Fe_2O_3 (Rhombohedral

277   hematite phase, JCPDS 00-001-1053) and/or CeO_2 (cubic phase, JCPDS

278   01-081-0792). As for the pure CeO_2 catalyst, the XRD patterns before and after

279   reaction showed similar crystal phases, although the crystallinity was increased after

280   experiments. While the peaks of pure Fe_2O_3 was totally disappeared, Fe_3O_4 (cubic

281   magnetite phase, JCPDS 00-001-1111) were observed after the redox reactions. It

282   might be attributed that the presence of reducing gases (e.g. H_2 and CO) reduced the

283   Fe_2O_3 catalysts into compounds such as Fe_3O_4 which was the active phase in water

284   gas shift process. While the metallic Fe^0 was not observed in the XRD patterns. It

285   might be owing to that the Fe^0 was oxidized to Fe_3O_4 by steam ($3Fe + 4H_2O$ (vapor) =

286    $Fe_3O_4 + 4H_2$), since the steam was fed to the system continuously. Fe^0 in iron oxygen

287   carrier could not be fully oxidized into Fe^{3+} with steam as oxidizing agent, this is in

288   agreement with Vozniuk's work [45]. Therefore, Fe_3O_4 was identified in the XRD

289   patterns of the used Fe_2O_3 catalyst after a series reaction as Fe_2O_3 → Fe_3O_4 → Fe →

290   Fe_3O_4.

291   In regard to fresh CeO_2/Fe_2O_3 bimetal catalysts, it was noticed that cerium and

292   iron did not form any binary metal oxides (Ce_xFe_yO), and no obvious phase changes

293   for Ce and Fe with the ratio of Ce:Fe changing. In addition, there were no cerium/iron

294   ions substituting into the cerium/iron lattice sites. Since the catalysts were calcined at

295   800 °C under air environment, Ce^{3+} ion was oxidized into Ce^{4+} ion, that's the reason

296   that the diffraction peaks of CeO_2 rather than Ce_2O_3 exist. With the decrease of the

297   ratio of Ce:Fe from 7:3 to 5:5 and then 3:7, the content of iron in the mixture was

298   increased. The diffraction of the fresh catalysts appears to be narrower and sharper

299   when the ratio of Ce:Fe was decreased. Furthermore, the diffraction peaks of Fe_2O_3

300   become more and more obvious especially in the Ce:Fe=3:7 catalyst. It is

301   demonstrated that the size of metal particles in the prepared catalysts was increased as

302   evaluated using the Scherrer Equation. In addition, the addition of Fe resulted in the

303   increase of the crystallinity and the size of Fe-based particles. It can be noticed that

304   the diffraction peaks of CeO_2 become narrower and sharper as the ratio of ceria in

305   Ce:Fe decreasing, that indicated the particle sizes of CeO_2 is increasing, it seems that

306   CeO_2 might be sintering when the amount of CeO_2 atoms is the minority(in this

307   experiment the ratio of Ce:Fe is 3:7).

308   For the used Ce/Fe catalysts, a perovskite type composite oxide $CeFeO_3$

309   (orthorhombic phase, JCPDS 00-022-0166) and Fe_3O_4 (cubic magnetite phase,

310   JCPDS 00-001-1111) were showed. It might be attributed that the presence of

311   reducing gases (e.g. H_2 and CO) reduced the catalysts into compounds such as Fe_3O_4

312   during the water-shifting process. The new perovskite phase $CeFeO_3$ was also formed

313   during the experiment and it has been proved that perovskite ferrite have high

314   capacity and mobility of oxygen, fast response time and high activity [38], which

315   might be favourable for cellulose gasification. Unlike only Fe_3O_4 peaks could be seen

316   in the used pure Fe_2O_3 catalyst, both Fe_2O_3 and Fe_3O_4 were observed in the used

317   Ce/Fe catalysts. It could be related to that the introducing of CeO_2 promoted the

318   oxidation of Fe_3O_4 to Fe_2O_3 in steam environment, because ceria has a high and multi

319   valence state and can undergo fast and reversible $Ce^{+3} \leftrightarrow Ce^{+4}$ transformation for

320   oxygen storing and releasing.

321   As shown in Fig. 2b, the $CeFeO_3$ peaks are much more obviously than that of

322   Fe_3O_4 and the peaks of Fe_2O_3 can't be seen especially at the ratio of Ce:Fe=7:3, i.e.,

323   Fe was mainly existed in the form of $CeFeO_3$ lattice. It is indicated that the Fe

324   element in the fresh catalysts was likely to form $CeFeO_3$ in used catalysts rather than

325   Fe_3O_4 or Fe_2O_3 after the redox reactions. With Fe ratio increasing, the diffraction peak

326   of Fe_3O_4 is becoming more significant, it can be related to the generated hydrogen and

327   carbon monoxide in-situ reduced the iron oxide and the iron-steam reaction ($Fe + H_2O$

328    $= Fe_3O_4 + H_2$). In return, it promoted the production of CO, H_2 and other gases as

329   shown in Table 1, because Fe_3O_4 was the active phase and had a high catalytic activity.

330   And the existence of $CeFeO_3$ was also beneficial to steam gasification of volatile

331   further increasing the gas production than that of pure Fe_2O_3 or CeO_2. The hydrogen

332   yield reached the maximum with the Ce:Fe=3:7 catalyst which shows strong

333   diffraction of $CeFeO_3$ and Fe_3O_4 in the XRD analysis.
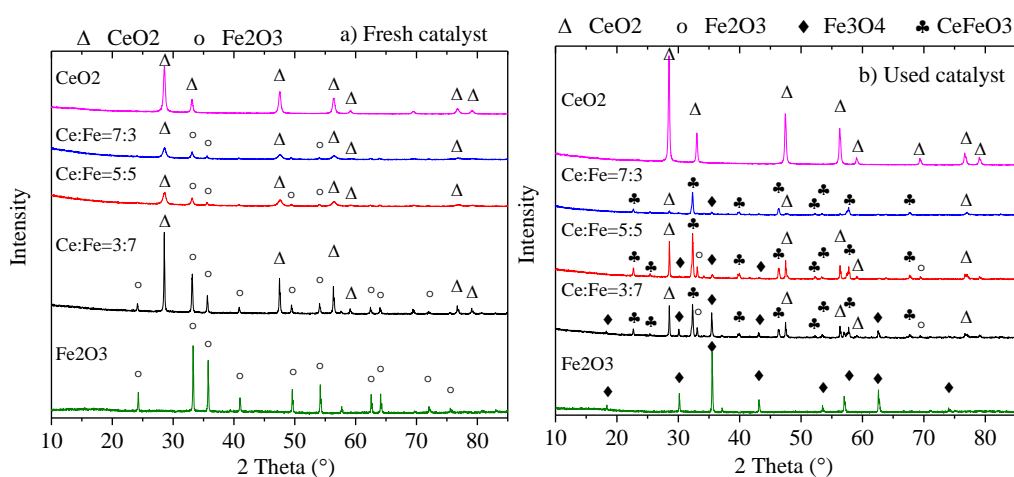
334

335   Figure 2. XRD patterns of catalysts with different Ce/Fe ratio.

336

337   3.1.3. TPR (Temperature programmed reduction) analysis

338   Fig. 3 shows the TPR profiles of catalyst reduction in relation to the reduction

339   stages and the corresponding temperature. For CeO_2, the reduction of CeO_2 to Ce_2O_3

340   shows two peaks, one quite weak peak at 511.2 ^{o}C as the surface shell reduction[27]

341   (as shown in Fig. 2S) and a relatively slight increase showed at higher temperature

342   (>700°C) for bulk reduction, it indicated that CeO_2 is very stable, and higher

343   temperature might lead to the reduction of CeO_2 to Ce_2O_3. While Fe_2O_3 showed good

344   reducibility, and the reduction process can be divided into 3 steps of reduction. The

345   reduction of Fe_2O_3 (hematite) to magnetite (Fe_3O_4) was located at ~467.9 ^{o}C, and is

346   followed by the reduction of magnetite (Fe_3O_4) to wustite (FeO) at 600 ^{o}C ~720 ^{o}C.

347   Further reduction of wustite to metallic Fe^0 happens at around 800 ^{o}C, while the

348   complete reduction of FeO to Fe^0 could not be observed. The process can be

349   described as the follows:

350   Fe_2O_3 (hematite) $\rightarrow$ Fe_3O_4 (magnetite) $\rightarrow$ FeO (wustite) $\rightarrow$ Fe
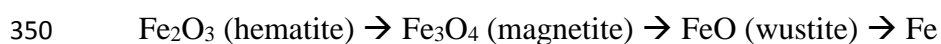
351   While the reduction of Fe_3O_4 to FeO as shown in Fig.3 was shifted to higher

352   temperature and mixed together with the reduction of FeO to Fe^0. It indicated that the

353   Fe_3O_4 was thermal sintering at high temperature and hard to be reduced, as reported in

354   other's work[46, 47].

355   Studies show that the reduction process significantly depends on the existence of

356   another metal oxide in the modified iron oxide[27, 31]. And that is confirmed in

357   Ce/Fe catalysts. For the mixture of CeO_2 and Fe_2O_3 (Ce：Fe=7：3), still three peaks are

358   showed: i) the reduction of hematite to magnetite at 455.9 ^{o}C which is similar with

359   that of pure Fe_2O_3; ii) followed by the reduction of magnetite to wustite which is

360   shifted to lower temperature as 668.8 $^{\circ}$C, it means that Fe_3O_4 is easier to be reduced to

361   FeO, which indicates that the presence of CeO_2 decreases the thermal sintering of

362   Fe_3O_4; iii) while the last peak was much wider than that of the reduction of wustite to

363   metallic Fe^0 for pure Fe_2O_3 catalyst, it might be the combination peaks of the

364   reduction of CeO_2 to Ce_2O_3 and FeO to Fe^0.

365   With the ratio of increasing of Fe (Ce:Fe=5:5), the TPR profile is similar to that

366   of Ce:Fe=7:3 except that the peak value is lowed and reducibility is weakened. While

367   with the ratio of Fe increasing further to Ce:Fe=3:7, the reduction of Fe_3O_4 to FeO

368   was shifted to high temperature as 706.6 $^{\circ}$C obviously, i.e., the reduction of Fe_3O_4

369   became difficult. It might be owing to that the preventing of Fe_3O_4 from thermal

370   sintering was weaken as the ratio of CeO_2 was lowered (Ce:Fe=3:7).

371   As can be seen in the TPR results, similar reduction peaks are obtained for Ce/Fe

372   catalysts and the catalyst with pure CeO_2 or Fe_2O_3. Therefore, the possible

373   intermediate cerium iron bimetallic species is not showed, it suggested that the

374   interaction between Fe and CeO_2 support was weak after the calcination during the

375   process of catalysts preparation. This is in good agreement with the XRD results.

376   However, the reducibility of the catalysts changes with the variation ratio of Ce:Fe,

377   the reducibility of $Ce_3Fe_7O_y$ is the strongest among the impregnation Ce/Fe catalysts

378   and surpassed only by pure Fe_2O_3, and the whole reduction profile of the CeO_2 shows

379   that the reducibility of CeO_2 is much less by orders of magnitude than the Ce/Fe

380   catalysts. This is in positive correlation with the ratio of iron. And the hydrogen

381   consumption of $Fe^{3+} \rightarrow Fe^0$ is 26.86 mmol g-1, much higher than that of $Ce^{4+} \rightarrow Ce^{3+}$

382   with the value of 3.57 mmol g-1.
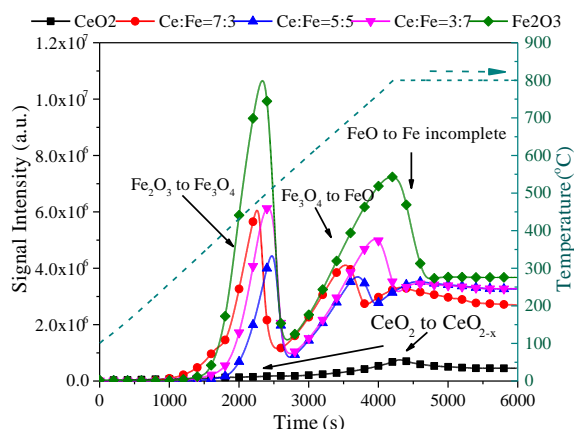
383

384   Figure 3. TPR profiles of fresh catalysts with different Ce/Fe ratio.

385

386   3.2 Lifetime test of the catalysts

387   In order to further investigating the performance of the catalysts during the

388   gasification of cellulose, the stability of catalysts was tested for 5 cycles (during each

389   cycle, fresh cellulose sample was introduced) with Ce:Fe=3:7 catalyst used   as the

390   catalyst showed the best performance in terms of hydrogen production. In addition,

391   the temperature was set as 800°C and the water feeding rate was 0.1 g min^{-1} for the

392   lifetime test. The gas yield was listed in in Table 2. It can be found that when the

393   catalyst was used for 1 and 2 times, the gas yield increased obviously and the content

394   of H_2 was kept steady, hence the yield of hydrogen increased gradually to 29.35 mmol

395   g-1 cellulose, the performance of catalyst seems to become better and it might be

396   owing to the existence of highly–active compounds such as Fe_3O_4 or $CeFeO_3$ after the

397   first redox experiment (as shown in Fig.4). However, with catalyst used further (over

398   3 times), the increasing trend become gentle and H_2 and CO yield decreased slightly,

399   but CH_4 and CO_2 increased slightly, although the increase of CO_2 (from 10.28 to

14.58 mmol g^{-1} cellulose) surpassed that of CH_4 (from 9.27 to 11.54 mmol g^{-1} cellulose) and occupied the main increment. It infers that the oxidation of catalyst might be increased and promote the formation of carbon dioxide. However, from the life test result, we can know that the yield of H_2 is still kept 26.29 mmol g-1 with H_2 content over 30% and CO about 40%. The heat value is kept at about 13 MJ $(Nm^3)^{-1}$. It indicated that the catalytic activity of the catalyst we used is still kept stable without obvious inactivation. It indicated that the performance of Ce:Fe=3:7 catalyst is not too bad for hydrogen production after five times reusing test.

Table 2. Gas yields in lifetime test for catalysts (Ce:Fe=3:7) stability.

Life time	1	2	3	4	5
Gas yield (wt.%)	84.64	88.94	90.99	91.50	91.98
Mass balance (%)	98.30	97.99	97.18	96.33	96.16
H2 yield (mmol g^{-1} cellulose)	28.58	29.35	28.12	27.31	26.29
Gas composition (vol.%)					
H_2	33.69	33.35	31.93	31.17	30.33
CO_2	12.12	14.23	15.32	15.95	16.81
CH_4	10.93	11.72	12.48	13.12	13.31
CO	43.26	40.70	40.27	39.75	39.54

The XRD spectra of used Ce/Fe catalyst is shown in Fig. 4. The XRD spectra of the catalyst used with variant cycles exhibit the same pattern. However, the diffraction peaks of CeO_2 and Fe_2O_3 become more and more significant while the patterns of $CeFeO_3$ and Fe_3O_4 seem to be weakened with the catalyst recycle except that there is an increasing of $CeFeO_3$ peak during the 2 times reusing. It is consistent with the catalytic activity as higher H_2 yield for catalyst reused for twice, it indicated that Ce_2FeO_3 is more active for water shifting reaction of biomass with more H_2 and

417 CO formed. The decrement of active compounds of $CeFeO_3$ and Fe_3O_4 resulted in the

418 weak performance of catalyst with catalyst reused further (recycle time over 3), while

419 the increment of CeO_2 and Fe_2O_3 promoted the oxidation of catalyst, and leading to

420 more CO_2 formed.
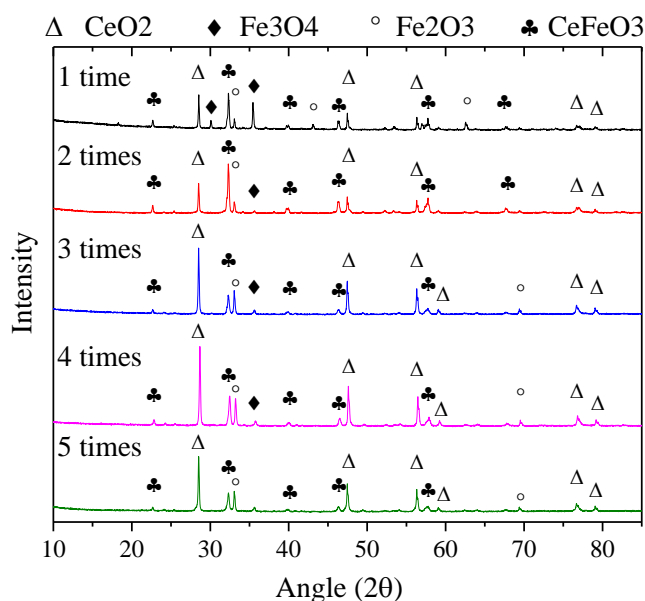
421

422   Figure 4. XRD patterns of reacted catalysts (Ce:Fe=3:7) after several times.

423   The morphologies of the used catalysts after each cycle were shown in Fig. 5.

424 The deposition of carbon on the surface of the reacted catalysts is difficult to be

425 observed as shown in Fig.5, as steam injecting during water-gas shifting process

426 might react with potential carbon deposition. With catalyst recycle going, some

427 irregular particles were observed on the surface of catalysts, it might be attributed to

428 the agglomeration generated at higher temperature (800 ^{o}C). Combined with the XRD

429 results of the reacted catalyst in Fig.4, it might be CeO_2 particles that were

430 agglomerated.

431

432
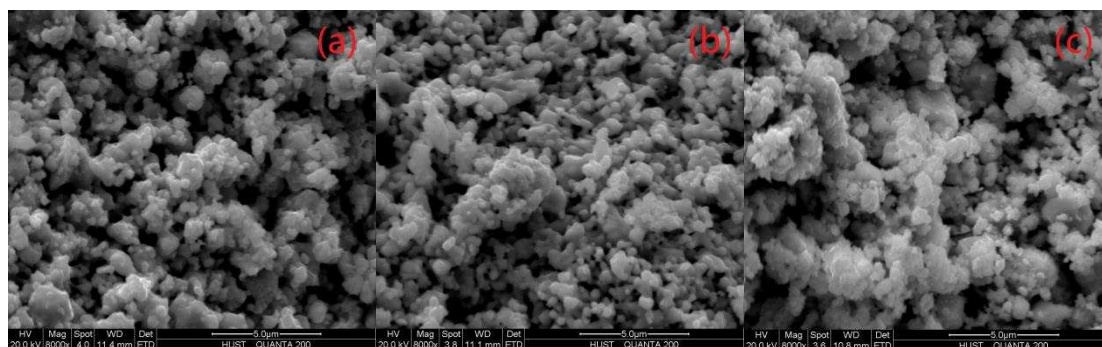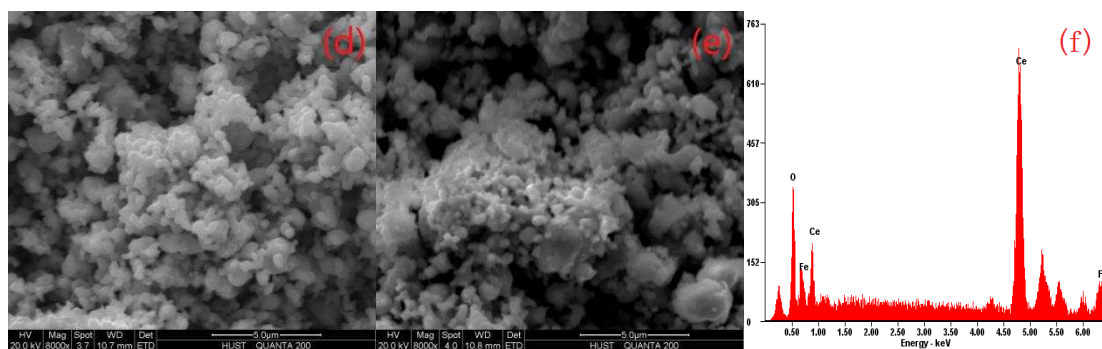
Figure 5. SEM micrographs of CexFeyO (x:y=3:7) after several tests. (a)~(e)

represents the catalysts reacted for one, two, three, four, five times respectively. (f)

EDX results for the reacted catalysts.

Possible carbon deposition on the used catalysts was carried out with TPO

analysis and the results were showed in Fig.6. The weight increased at 250 ^{o}C to 550

^{o}C, it might be caused by the oxidation of metallic Fe (a few of Fe particles exist

possibly, cannot be seen in XRD patterns in Fig.4) and Fe_3O_4 to Fe_2O_3. With the

increase of recycle times, the weight gaining of used catalysts shown in Fig.6 was

decreased. As part of the Fe_3O_4 was oxidized to Fe_2O_3 in the lifetime test as shown in

Fig.4. Therefore it cost less oxygen in the TPO test and resulted in less weight gain.

As for the oxidation peak shifting to higher temperature, it might be ascribed to the

thermal sinter of Fe_3O_4 particles after each recycle, which made Fe_3O_4 hard to be

oxidized. However, the weight loss peak can be hardly seen in TPO analysis, only a

446   slight decrement was around 550 °C, it might be the oxidation of filamentous carbon

447   [11, 48] and there was no amorphous carbon oxidizing peak. Generally speaking, the

448   carbon deposition on catalysts was trace amounts and could be neglected. It seems

449   that the presence of CeO_2 not only improved the oxidative ability of the iron catalysts,

450   but was also in favour of the oxidation of possible deposited carbon on the surface of

451   the used catalysts, because the CeO_2 has a high capacity and mobility of oxygen.
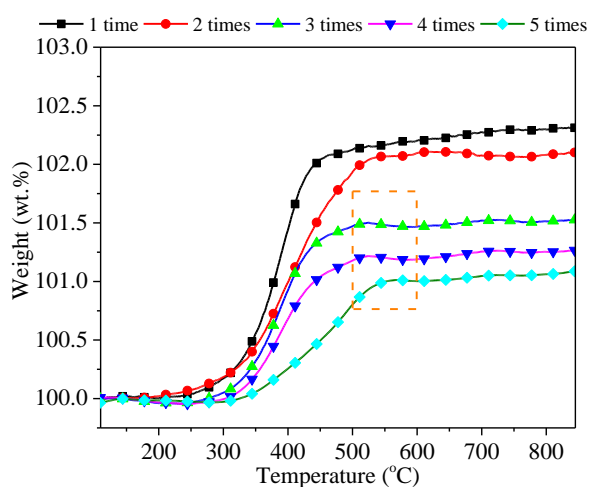
452

453   Figure 6. Temperature programmed oxidation of used catalysts after several

454   recycles.

455

456   3.3 Influence of reaction temperature

457   The influence of catalytic temperature on the hydrogen production from biomass

458   gasification was investigated, when cellulose pyrolysis temperature was kept at 800

459   °C and the water feeding rate was 0.1 g min^{-1} in the presence of the catalyst

460   (Ce:Fe=3:7), while the gasification temperature varied from 500 °C to 900 °C at the

461   step of 100 °C. As can be seen in Table 3, the gas yield was increased straightly from

462   62.92 wt.% to 85.84 wt.%, which indicated that the gasification temperature had a

463 significant effect on the thermal conversion of liquid oil compounds to light gases.

464 For that gas product, the concentrations of hydrogen and carbon oxide increased

465 slightly as temperature increasing from 500°C to 700°C, while the content of methane

466 decreased straightly from 16.95 vol.% to 12.24 vol.%, but no obvious change showed

467 for carbon monoxide. This can be explained by that the increase of temperature

468 restrained the production of CH_4 while promoted the water gas shift reaction (CO +

469 $H_2O = CO_2 + H_2$). When the temperature was further increased to 800 $^{\circ}$C, the yield of

470 hydrogen reached the maximum at 28.58 mmol and the concentration of CO was

471 increased significantly to 43.26 vol.%. These can be attributed to that the cracking

472 reactions and catalytic steam reforming of volatiles were enhanced with the increase

473 of reaction temperature. While at 900 $^{\circ}$C, the yields of CO_2 and H_2 were decreased

474 while the yield of CO was increased at higher temperature, it might be iron's role on

475 reversed water gas shift ($CO_2 + H_2 = CO + H_2O$) prevail over the former at elevated
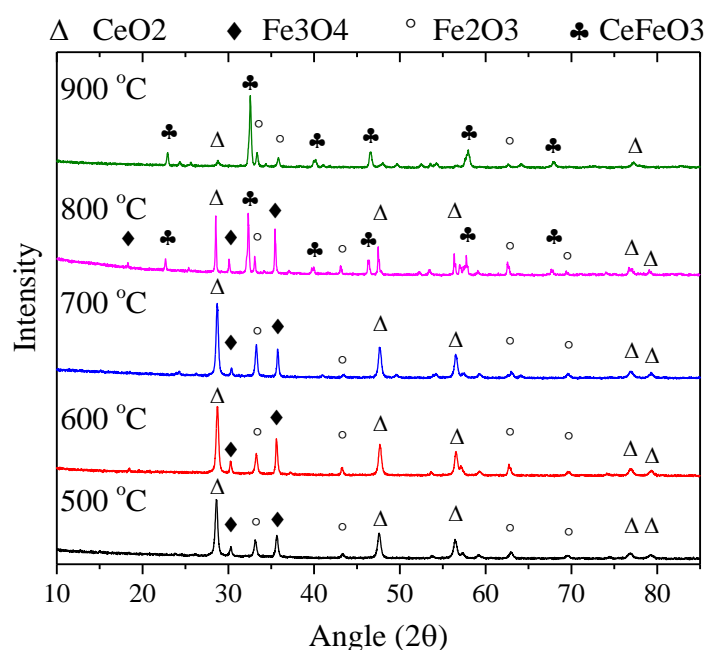
476 temperature.

477   Table 3. The influence of gasification temperature on gas production.

Different gasification temperature ($^{\circ}$C)	500	600	700	800	900
Gas yield (wt.%)	62.92	67.69	72.94	84.64	85.84
Mass balance (%)	102.92	99.53	97.01	98.30	97.88
H2 yield (mmol g^{-1} cellulose)	18.77	21.36	24.03	28.58	27.01
Gas composition (vol.%)					
H_2	30.56	32.78	33.86	33.69	31.57
CO_2	15.33	17.64	17.56	12.12	11.23
CH_4	16.95	12.78	12.24	10.93	12.81
CO	37.16	36.80	36.35	43.26	44.40

478

479   Fig. 7 shows the results of XRD analysis of the used catalysts obtained at

different reaction temperatures. After used at 500 °C, a diffraction peak of Fe_3O_4 was showed with some Fe_2O_3 and CeO_2. With gasification temperature increasing from 500 to 700 °C, the diffraction peak of Fe_3O_4 was increasing while the Fe_2O_3 patterns decreased; it indicated that proper high temperature was benefit for the reduction of Fe_2O_3 to Fe_3O_4. It should be notice that some $CeFeO_3$ patterns showed at 800 °C, while Fe_2O_3 and CeO_2 diminished. And when the temperature reached 900 °C, the diffraction of $CeFeO_3$ becomes more remarkable while the diffraction patterns of Fe_3O_4 was disappeared. The peak of CeO_2 become weak and they are mainly existed in $CeFeO_3$ with trace Fe_2O_3. It indicates that temperature was an important factor for the formation of $CeFeO_3$; CeO_2 would agglomerated with Fe_2O_3 and formed $CeFeO_3$ at higher temperature. The decrease of the diffraction of Fe_3O_4 might be due to the following two reasons; 1) More Fe ions were used to form $CeFeO_3$ lattice. 2) The oxidation of Fe_3O_4 to Fe_2O_3 was enhanced at higher temperature.

Figure 7. XRD patterns of used catalysts (Ce:Fe=3:7) under different temperature.

495

4. Conclusions

The present study introduced Ce/Fe catalyst into the biomass steam gasification. The influences of mole ratio of Ce:Fe and catalytic temperature on hydrogen production were investigated in a two stage gasification system. The main conclusions are listed as the follows. The CeO_2/Fe_2O_3 catalyst with a Ce:Fe ratio of 3:7 is optimal for the hydrogen production in cellulose steam gasification. When the temperature increased from 500 ^{o}C to 900 ^{o}C, the catalyst promoted the volatile steam gasification and resulted in the increasing of gas yield. However the highest hydrogen production was 28.58 mmol g-1 cellulose at 800 ^{o}C owing to that the iron enhanced the reversed water shift reaction at 900 ^{o}C and caused the decreasing of hydrogen and carbon monoxide. $CeFeO_3$ can be generated at 800 ^{o}C or higher temperature after steam gasification of biomass without forming CeO_2/Fe_2O_3 clathrate. And the existence of $CeFeO_3$ enhanced the thermal stability of Ce/Fe catalyst. The increase of iron addition resulted in an enhancement of the crystallinity and the particle size of the used catalyst. The decrease of $CeFeO_3$ and Fe_3O_4 rather than the agglomeration of CeO_2 or carbon deposition is the main reason that deactivated the catalysts in the lifetime test. The presence of CeO_2 not only improved the oxidative ability of the iron catalysts, but was also promoted the oxidation of possible deposited carbon on the surface of the used catalysts due to the high capacity and mobility of oxygen in CeO_2.

515

522

523   References

524   [1] M. Pehnt. Assessing future energy and transport systems: The case of fuel cells -
525   Part 2: Environmental performance. International Journal of Life Cycle Assessment. 8
526   (2003) 365-78.
527   [2] G. Chen, J. Andries, H. Spliethoff. Catalytic pyrolysis of biomass for hydrogen
528   rich fuel gas production. Energy Conversion and Management. 44 (2003) 2289-96.
529   [3] L.H. Zhang, C.B. Xu, P. Champagne. Overview of recent advances in
530   thermo-chemical conversion of biomass. Energy Conversion and Management. 51
531   (2010) 969-82.
532   [4] J. Li, Y.Q. Chen, H.P. Yang, D.C. Zhu, X. Chen, X.H. Wang, et al. Correlation of
533   Feedstock and Bio-oil Compound Distribution. Energy & Fuels. 31 (2017) 7093-100.
534   [5] E. Shayan, V. Zare, I. Mirzaee. Hydrogen production from biomass gasification; a
535   theoretical comparison of using different gasification agents. Energy Conversion and
536   Management. 159 (2018) 30-41.
537   [6] W.N. Li, Q.H. Li, R. Chen, Y. Wu, Y.G. Zhang. Investigation of hydrogen
538   production using wood pellets gasification with steam at high temperature over 800
539   degrees C to 1435 degrees C. International Journal of Hydrogen Energy. 39 (2014)
540   5580-8.
541   [7] H.Y. Chu, Q.H. Li, A.H. Meng, Y.G. Zhang. Investigation of hydrogen production
542   from model bio-syngas with high CO2 content by water-gas shift reaction.
543   International Journal of Hydrogen Energy. 40 (2015) 4092-100.
544   [8] T. Tian, Q.H. Li, R. He, Z.C. Tan, Y.G. Zhang. Effects of biochemical composition
545   on hydrogen production by biomass gasification. International Journal of Hydrogen
546   Energy. 42 (2017) 19723-32.
547   [9] J.G. Olsson, J.B. Pettersson, N. Padban, I. Bjerle. Alkali metal emission from filter
548   ash and fluidized bed material from PFB gasification of biomass. Energy & fuels. 12
549   (1998) 626-30.
550   [10] C. Wu, P.T. Williams. Hydrogen production by steam gasification of
551   polypropylene with various nickel catalysts. Applied Catalysis B-Environmental. 87
552   (2009) 152-61.
553   [11] C. Wu, P.T. Williams. Investigation of Ni-Al, Ni-Mg-Al and Ni-Cu-Al catalyst

for hydrogen production from pyrolysis-gasification of polypropylene. Applied Catalysis B-Environmental. 90 (2009) 147-56.

[12] C.F. Wu, P.T. Williams. Hydrogen Production from the Pyrolysis-Gasification of Polypropylene: Influence of Steam Flow Rate, Carrier Gas Flow Rate and Gasification Temperature. Energy & Fuels. 23 (2009) 5055-61.

[13] L.Y. Wei, H.P. Yang, B. Li, X.T. Wei, L. Chen, J.G. Shao, et al. Absorption-enhanced steam gasification of biomass for hydrogen production: Effect of calcium oxide addition on steam gasification of pyrolytic volatiles. International Journal of Hydrogen Energy. 39 (2014) 15416-23.

[14] C. Wu, Z. Wang, J. Huang, P.T. Williams. Pyrolysis/gasification of cellulose, hemicellulose and lignin for hydrogen production in the presence of various nickel-based catalysts. Fuel. 106 (2013) 697-706.

[15] P.H. Blanco, C. Wu, P.T. Williams. Influence of Ni/SiO2 catalyst preparation methods on hydrogen production from the pyrolysis/reforming of refuse derived fuel. International Journal of Hydrogen Energy. 39 (2014) 5723-32.

[16] N. Laosiripojana, W. Sutthisripok, S. Charojrochkul, S. Assabumrungrat. Conversion of biomass tar containing sulphur to syngas by GdCeO2 coated NiFe bimetallic-based catalysts. Applied Catalysis A: General. 478 (2014) 9-14.

[17] A. Laobuthee, C. Veranitisagul, W. Wattanathana, N. Koonsaeng, N. Laosiripojana. Activity of Fe supported by Ce1−xSmxO2−δ derived from metal complex decomposition toward the steam reforming of toluene as biomass tar model compound. Renewable Energy. 74 (2015) 133-8.

[18] S.W. Luo, L. Zeng, L.S. Fan. Chemical Looping Technology: Oxygen Carrier Characteristics. in: J.M. Prausnitz, (Ed.). Annual Review of Chemical and Biomolecular Engineering, Vol 6. Annual Reviews, Palo Alto, 2015. pp. 53-75.

[19] M. Keller, H. Leion, T. Mattisson, H. Thunman. Investigation of Natural and Synthetic Bed Materials for Their Utilization in Chemical Looping Reforming for Tar Elimination in Biomass-Derived Gasification Gas. Energy & Fuels. 28 (2014) 3833-40.

[20] M. Keller, H. Leion, T. Mattisson. Use of CuO/MgAl2O4 and La0.8Sr0.2FeO3/γ-Al2O3 in chemical looping reforming system for tar removal from gasification gas. Aiche J.   (2015).

[21] M. Keller, H. Leion, T. Mattisson. Chemical looping tar reforming using La/Sr/Fe-containing mixed oxides supported on ZrO2. Applied Catalysis B: Environmental. 183 (2016) 298-307.

[22] G. Chen, J. Yao, J. Liu, B. Yan, R. Shan. Biomass to hydrogen-rich syngas via catalytic steam gasification of bio-oil/biochar slurry. Bioresource Technology. 198 (2015) 108-14.

[23] Z. Huang, F. He, Y.P. Feng, K. Zhao, A.Q. Zheng, S. Chang, et al. Synthesis gas production through biomass direct chemical looping conversion with natural hematite as an oxygen carrier. Bioresource Technology. 140 (2013) 138-45.

[24] C. Lang, X. Secordel, Y. Zimmermann, A. Kiennemann, C. Courson. High-temperature Water–Gas Shift catalysts for hydrogen enrichment of a gas produced by biomass steam gasification. Comptes Rendus Chimie. 18 (2015) 315-23.

598 [25] G.K. Reddy, S.J. Kim, J.H. Dong, P.G. Smirniotis, J.B. Jasinski. Long-term WGS
599 stability of Fe/Ce and Fe/Ce/Cr catalysts at high and low steam to CO ratios-XPS and
600 Mossbauer spectroscopic study. Applied Catalysis a-General. 415 (2012) 101-10.
601 [26] S. Cocchi, M. Mari, F. Cavani, J.-M.M. Millet. Chemical and physical behavior
602 of $CoFe_2O_4$ in steam–iron process with methanol. Applied Catalysis B:
603 Environmental. 152–153 (2014) 250-61.
604 [27] A. Khan, P. Chen, P. Boolchand, P.G. Smirniotis. Modified nano-crystalline
605 ferrites for high-temperature WGS membrane reactor applications. J Catal. 253 (2008)
606 91-104.
607 [28] K. Svoboda, G. Slowinski, J. Rogut, D. Baxter. Thermodynamic possibilities and
608 constraints for pure hydrogen production by iron based chemical looping process at
609 lower temperatures. Energy Conversion and Management. 48 (2007) 3063-73.
610 [29] M. Rafati, L.J. Wang, D.C. Dayton, K. Schimmel, V. Kabadi, A. Shahbazi.
611 Techno-economic analysis of production of Fischer-Tropsch liquids via biomass
612 gasification: The effects of Fischer-Tropsch catalysts and natural gas co-feeding.
613 Energy Conversion and Management. 133 (2017) 153-66.
614 [30] K.S. Kang, C.H. Kim, W.C. Cho, K.K. Bae, S.W. Woo, C.S. Park. Reduction
615 characteristics of $CuFe_2O_4$ and Fe_3O_4 by methane; $CuFe_2O_4$ as an oxidant for
616 two-step thermochemical methane reforming. International Journal of Hydrogen
617 Energy. 33 (2008) 4560-8.
618 [31] G.K. Reddy, P. Boolchand, P.G. Smirniotis. Unexpected Behavior of Copper in
619 Modified Ferrites during High Temperature WGS Reaction—Aspects of Fe^{3+} ↔
620 Fe^{2+} Redox Chemistry from Mössbauer and XPS Studies. J Phys Chem C. 116 (2012)
621 11019-31.
622 [32] S.B. Bagherzadeh, M. Haghighi, N. Rahemi. Novel oxalate gel coprecipitation
623 synthesis of ZrO_2-CeO_2-promoted CuO-ZnO-Al_2O_3 nanocatalyst for fuel cell-grade
624 hydrogen production from methanol: Influence of ceria-zirconia loading. Energy
625 Conversion and Management. 134 (2017) 88-102.
626 [33] D.H. Lee, K.S. Cha, Y.S. Lee, K.S. Kang, C.S. Park, Y.H. Kim. Effects of CeO_2
627 additive on redox characteristics of Fe-based mixed oxide mediums for storage and
628 production of hydrogen. International Journal of Hydrogen Energy. 34 (2009)
629 1417-22.
630 [34] D. Yamaguchi, L.G. Tang, L. Wong, N. Burke, D. Trimm, K. Nguyen, et al.
631 Hydrogen production through methane-steam cyclic redox processes with iron-based
632 metal oxides. International Journal of Hydrogen Energy. 36 (2011) 6646-56.
633 [35] Science-News. 2013 Runners-Up. Newcomer juices up the race to harness
634 sunlight. Science. 342 (2013) 1438-9.
635 [36] Nature-News-Features. 365 days: Nature's 10: Ten people who mattered this
636 year-Henry Snaith: Sun worshipper. Nature. 504 (2013) 357-65.
637 [37] A.M. Hafez, A.F. Zedan, S.Y. AlQaradawi, N.M. Salem, N.K. Allam.
638 Computational study on oxynitride perovskites for CO_2 photoreduction. Energy
639 Conversion and Management. 122 (2016) 207-14.
640 [38] N.X. Lin, L.N. Huo, H.P. Liu, X. Fang, S.T. Wu, X. Chen, et al. Preparation and
641 properties of pure crystalline perovskite $CeFeO_3$ thin films with vanadium doping. J

Am Ceram Soc. 100 (2017) 2932-8.

[39] E.A. Zaboeva, S.G. Izotova, V.I. Popkov. Glycine-Nitrate Combustion Synthesis of CeFeO3-based Nanocrystalline Powders. Russ J Appl Chem+. 89 (2016) 1228-36.

[40] L.L. Petschnig, G. Fuhrmann, D. Schildhammer, M. Tribus, H. Schottenberger, H. Huppertz. Solution combustion synthesis of CeFeO3 under ambient atmosphere. Ceram Int. 42 (2016) 4262-7.

[41] N.R. Manwar, R.G. Borkar, R. Khobragade, S.S. Rayalu, S.L. Jain, A.K. Bansiwal, et al. Efficient solar photo-electrochemical hydrogen generation using nanocrystalline CeFeO3 synthesized by a modified microwave assisted method. International Journal of Hydrogen Energy. 42 (2017) 10931-42.

[42] T.R. Sahoo, M. Armandi, R. Arletti, M. Piumetti, S. Bensaid, M. Manzoli, et al. Pure and Fe-doped CeO2 nanoparticles obtained by microwave assisted combustion synthesis: Physico-chemical properties ruling their catalytic activity towards CO oxidation and soot combustion. Applied Catalysis B-Environmental. 211 (2017) 31-45.

[43] J. Zou, H. Yang, Z. Zeng, C. Wu, P.T. Williams, H. Chen. Hydrogen production from pyrolysis catalytic reforming of cellulose in the presence of K alkali metal. International Journal of Hydrogen Energy. 41 (2016) 10598-607.

[44] J. Wang, C.Y. Han, X.Y. Gao, J.C. Lu, G.P. Wan, D.D. He, et al. Rapid synthesis of Fe-doped CuO-Ce(0.8)Zro(0.2)O(2) catalysts for CO preferential oxidation in H-2-rich streams: Effect of iron source and the ratio of Fe/Cu. Journal of Power Sources. 343 (2017) 437-45.

[45] O. Vozniuk, S. Agnoli, L. Artiglia, A. Vassoi, N. Tanchoux, F. Di Renzo, et al. Towards an improved process for hydrogen production: the chemical-loop reforming of ethanol. Green Chemistry. 18 (2016) 1038-50.

[46] A. Khan, P.G. Smirniotis. Relationship between temperature-programmed reduction profile and activity of modified ferrite-based catalysts for WGS reaction. J Mol Catal a-Chem. 280 (2008) 43-51.

[47] L.F. Zhang, Y.X. Wu. Sol-Gel Synthesized Magnetic MnFe2O4 Spinel Ferrite Nanoparticles as Novel Catalyst for Oxidative Degradation of Methyl Orange. J Nanomater. 2013 (2013).

[48] D.D. Yao, Y.S. Zhang, P.T. Williams, H.P. Yang, H.P. Chen. Co-production of hydrogen and carbon nanotubes from real-world waste plastics: Influence of catalyst composition and operational parameters. Applied Catalysis B-Environmental. 221 (2018) 584-97.